ISSN NO: 2770-0003
March 2024

Nonlinear Optical Materials of Inorganic−Organic Hybrid Semiconductors (R− $C_6H_4CHCH_3NH_3)_2PbI_4$

Yuldasheva N.N., Qodamboyev.P.Q[1]., Mukhammadaliev.Kh.G[2]., Samandarov.E.Sh[1].
Khorezm Mamun Academy[1]
Institute of General and Inorganic Chemistry of Uzbekistan Academy of Sciences[2]

Abstract. This study presents the synthesis, crystal structure, and optical properties of two-dimensional (2D) layered inorganic-organic (IO) hybrid semiconductors, namely $(R\text{-}C_6H_4C_2H_4NH_3)_2PbI_4$, where R can be either CH_3 or Cl. These compounds exhibit a natural self-assembly.Synthesis of the nonlinear optical materialls of Inorganic−Organic Hybrid Semiconductors of $(Cl\text{-}C_6H_4\text{-}C_2H_4\text{-}NH_3)_2PbI_4$ with PbJ_4 salt, study of its composition and structure by physical research methods.

$(RNH_3)^+$ moieties sandwiched between two infinite 2D layers of the $[PbI_6]^{4-}$ octahedral network, resembling IO multiple quantum wells. The CH_3 compound crystallizes in an orthorhombic system in the $C_{mc}2_1$ space group, while the Cl compound crystallizes in a monoclinic system in the $P2_1/c$ space group. When fabricated as thin films, both compounds exhibit good orientation along the (100) direction. Single crystals and thin films of these compounds display strong Mott-type exciton features at room temperature, which are highly influenced by the self-assembly and crystal packing. The confined excitons, residing within the lowest band gap of the inorganic material, exhibit distinct photoluminescence peaks under one- and two-photon excitation. The perfectly aligned 2D self-assembly generates free excitons, while the locally crumpled layered arrangement leads to energy down-shifted excitons.

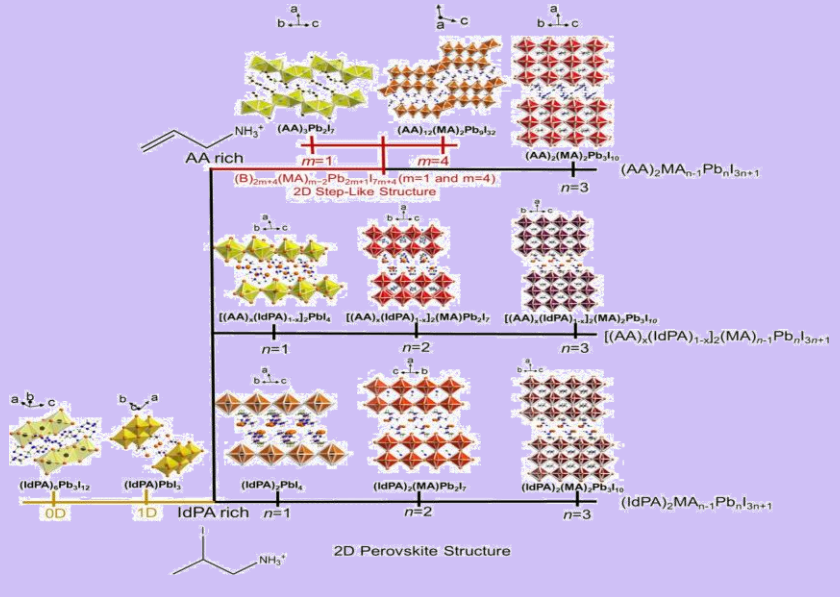

This study successfully presents the structural aspects of these novel IO hybrids and highlights the various differences in their physical and optical properties.

Scientific news. Inorganic−organic (IO) naturally self-assembled hybrid systems have been a fascinating subject of interest for many years because of their strong room-temperature excitons with high oscillator strength,[1–3] interesting structural features,[4-7] magnetic properties,[8] and promising electrical aspects.[9–11] The self-assembled systems from the class of $(RNH_3)_2MX_4$ (R= organic) are special and considered as natural multiple quantum well (MQW) structures where two $(RNH_3)^+$ moieties are sandwiched between two infinitely extended layers of $[MX_6]^{4-}$ octahedral. These two-dimensional (2D) IO hybrids show strong Mott type excitons within the MX_6 network. As a result of dielectric contrast and quantum confinement-related effects,[12] the exciton binding energies are enhanced larger than 200 meV.[13] The band gap tunability can be conveniently achieved from ~2 to ~3.2 eV by changing divalent metal halide (MX_2) inorganic entities alone (where M = Pb^{2+}, Mn^{2+},Sn^{2+}, Ge^{2+}, Eu^{2+},

ISSN NO: 2770-0003
March 2024

Cu^{2+}, Ni^{2+}, Fe^{2+}, and X = F^-,Cl^-, Br^- , I^-).[20–23] Such synergy between inorganic and organic has produced a great promising effect that led to the demonstration of many applications, namely, LEDs,[27]FETs,[21-22] solar cells, polariton lasers,[12-15] optical switches,[20-24] electro-optical modulators,[16] and so on. While the 2D crystal packing from RMX_3-type group entities is the most common, the organic moiety $(R{-}NH_3)^+$ conformation within the MX_2 network may lead to other dimensionalities depending on the type of the organic moiety, size, shape, and amino group location.[9-11]

Results. Recently, it is well explored that the structural influence of the organic moiety in 2D IO hybrids $(RNH_3)_2PbI_4$ (R = organic) directly influences the Pb−I−Pb crumpling angles and eventually band gap changes which directly reflects in the exciton energies.[23-24] In this communication, we have studied the synthesis, crystal structure.

Key words:, $(CH_3{-}C_6H_4{-}C_2H_4NH_3)_2PbI_4$ (MPEPI) and (Cl-C_6H_4-C_2H_4-$NH_3)_2PbI_4$ (CEPI) the crystallographic, thermal, and optical studies are systematically performed and present, biological activity, 3d metal, infrared spectroscopy, ultraviolet spectroscopy, X-ray diffraction.

Introduction: room-temperature exciton features in the 2D IO hybrid semiconductors, $(CH_3{-}C_6H_4{-}C_2H_4NH_3)_2PbI_4$ (MPEPI) and (Cl-C_6H_4-C_2H_4-$NH_3)_2PbI_4$ (CEPI) (Table 1). For both, the crystallographic, thermal, and optical studies are systematically performed and presented here. A critical comparison of MPEPI and CEPI is reported in this paper the inorganic network.

Table 1. **Empirical Names and Chemical Formulae of the Synthesized IO-Hybrids**

s. no.	empirical name	chemical formula
1.	1-(4-chlorophenyl) ethylammonium tetraiodoplumbate (CEPI)	$(Cl{-}C_6H_4{-}C_2H_4NH_3)_2PbI_4$
2.	1-(4-methylphenyl) ethylammonium tetraiodoplumbate (MPEPI)	$(CH_3{-}C_6H_4{-}C_2H_4NH_3)_2PbI_4$

Here, we focus on linear (onephoton induced, $\hbar\omega \geq$ Eg) and nonlinear (two-photoninduced, $2\hbar\omega \geq$ Eg) optical excitations to study various possible exciton energies that are possible in these 2D-aligned single crystals.[21] One-photon absorption (1PA, $\hbar\omega \geq$ Eg) due to high absorption coefficients results into quite small penetration depths (~1/α0),[22] therefore, conventional photoluminescence (1PA-PL) provides information only from the near-surfaces and are influenced by many unwanted effects such as background emission, photo-bleaching, ablation, laser heating effects, and so forth.[23] On the other hand, two-photon absorption (2PA) is a well-known third-order nonlinear effect which utilizes two infrared photons ($2\hbar\omega \geq$ Eg) and undergoes an electronic transition from the ground state to the excited state through an intermediate virtual state within the band gap. CEPI crystallizes into the monoclinic system in the space group $P2_1/c$, whereas MPEPI crystallizes into the orthorhombic system in $Cmc2_1$ space group. The unit cell dimensions of MPEPI are a = 32.544 Å; b = 9.316 Å; c = 8.6028 Å and $\alpha = \beta = \gamma = 90°$; on the other hand, the cell dimensions of CEPI are a = 16.200 Å; b = 9.2695 Å; c = 8.6314 Å and β = 96.738°. For MPEPI, the Pb−I−Pb bond angle is 147.27°; I−Pb−I bond angles are 84.17, 90.98, 95.86, and 88.2°; Pb−I bond lengths are in the range of 3.159 and 3.336 Å; C−C bond lengths are in the range of 1.350 and 1.536 Å; the C−N bond length is 1.529 Å. In case of CEPI, the Pb−I− Pb bond angle is 153.72°; I−Pb−I bond angles are 93.83, 86.14, 85.48, and 94.52°; Pb−I bond lengths are 3.285 and 3.232 Å; C−C bond lengths are in the range of 1.360−1.511 Å; the C−Cl bond length is 1.747 Å; and the C−N bond length is 1.507 Å. Both the structures consist of 2D alternate layers of PbI_6 and organic ammonium. This alternate layer fashion contains a double layer of protonated organic ammonium cations which are being sandwiched between infinitely extending PbI_6 sheets as shown in Figure 1. Layers are infinetely extended by corner-sharing distorted PbI_6 octahedra with the neighboring four octahedra through double-bridging iodine atoms. The complete crystallographic data of both MPEPI and CEPI are given in the Supporting Information (Table S1).

ISSN NO: 2770-0003
March 2024

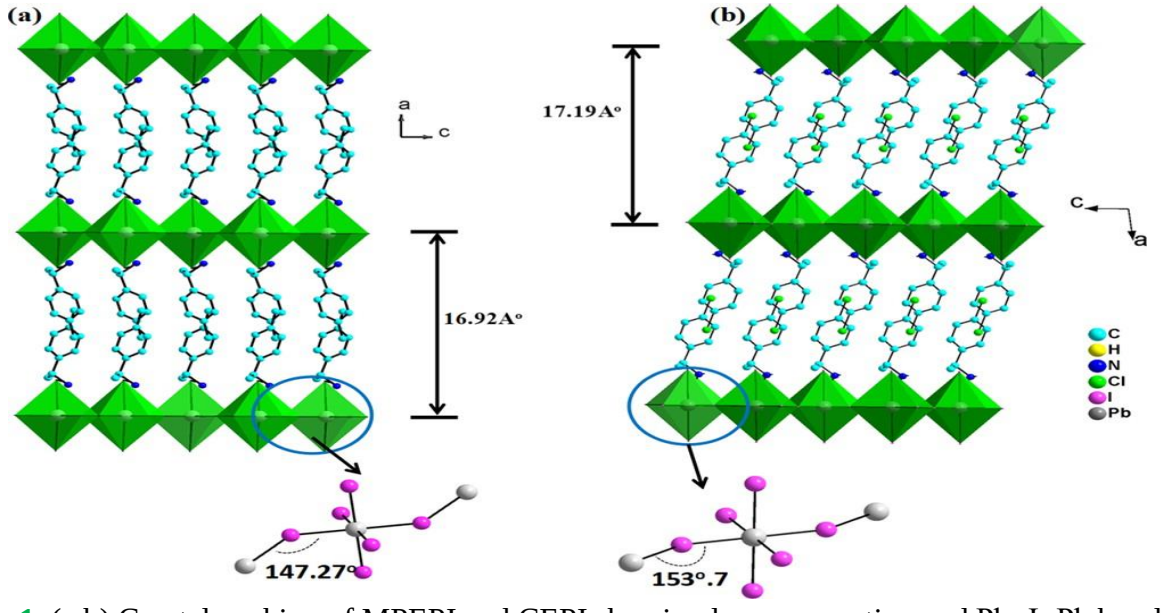

Figure 1. (a,b) Crystal packing of MPEPI and CEPI showing layer separation and Pb−I−Pb bond angle, respectively. (Hydrogens are omitted for clarity).

The separation between the infinitely extended lead iodide sheets is found to be 16.92 and 17.19 Å in MPEPI and CEPI, respectively. This difference can be attributed to the difference in the π–π and C−H–π interactions between the phenyl rings having different chemical environments around them. In both the crystal structures, the PbI_6 octahedra are slightly tilted because of in-plane Pb−I−Pb bond crumpling. This is observed to be ∼153.7 and ∼147.27° in CEPI and MPEPI, respectively.

Methods and materials. MPEPI and CEPI are prepared by conventional solution processing techniques.[23-25] In both the cases, stoichiometric quantities of organic [1-(4-methylphenyl) ethylamine or 1-(4- chlorophenyl) ethylamine] and lead (II) iodide (PbI_2) were taken in HI (55%) separately and stirred thoroughly to get clear solutions. These two solutions were mixed together slowly with constant stirring. The resultant precipitation is separated and dried properly. Both MPEPI and CEPI are dissolved in the acetonitrile solvent to get a saturated solution. Slow evaporation of saturated solution left dark yellow-colored crystal platelets and pale yellow rodlike crystals for CEPI and MPEPI, respectively. Suitable crystals are selected for single crystal analysis and optical studies.

Single crystal X-ray diffraction. Single crystal X-ray diffraction studies were carried out on BRUKER AXS SMART-APEX diffractometer with a CCD area detector (Mo Kα = 0.71073 Å, monochromator = graph- ite).[13-17] The thin films of MPEPI and CEPI are prepared by the spin-coating technique (typically at 3000 rpm resulting in the uniform film thickness of 120 nm), dissolving crystals in the acetonitrile solvent at a temperature slightly below room temperature. These thin films are used for glancing angle X-ray Diffraction (GAXRD) using Cu Kα (1.5418 Å) radiation. Absorption spectra are recorded using a Shimadzu UV-VIS- NIR3600 spectrometer. Thermo gravimetry (TG) was carried out between 25 and 800 °C at a scan rate of 5 °C/min under N_2 atmosphere using Al_2O_3 as the reference material. One- and two-photon absorption-induced photoluminescence (1PA-PL and 2PA-PL) was performed using 400 nm CW diode laser and high-intensity femtosecond Ti:Sapphire mode-locked oscillator laser (Spectra-Physics; MaiTai, tunable between 690 and 1040 nm, repetition rate = 84 MHz and pulse duration = 120 fs.). For 1PA-PL excitation, the sources are either from 400 nm CW diode laser or 400 nm (frequency doubled 800 nm) fs1 laser. High-resolution PL images, PL spatial spectral mapping of CEPI and MPEPI single crystals were carried out using an optical upright microscope (BX51, Olympus) by using above lasers. Spatial mapping was carried out by a controlled motorized *X*−*Y* stage attached with the microscope. The fiber optic-coupled spectrometer (Ocean Optics; QEPro) is used to collect the spectra through appropriate high and low pass filters.

Figure .This sort of bonding helps in rigid confirmation of the sensitive organic part of the IO hybrid system.It is interesting to compare with the previous studies[25] of similar hybrids formed by organic moieties, 4-X−$C_6H_4NH_2$, where X = Cl or CH_3O. When chloro-aniline is substituted as the organic moiety, the organic−inorganic hybrid assembles as a 2D-layered network [$(Cl{-}C_6H_4NH_3)_2PbI_4$], whereas for methoxy−aniline, the resultant network is

ISSN NO: 2770-0003
March 2024

composed of 1D PbI ribbons as $[(CH_3O{-}C_6H_4NH_3)_2Pb_3I_8{\cdot}2H_2O]$.

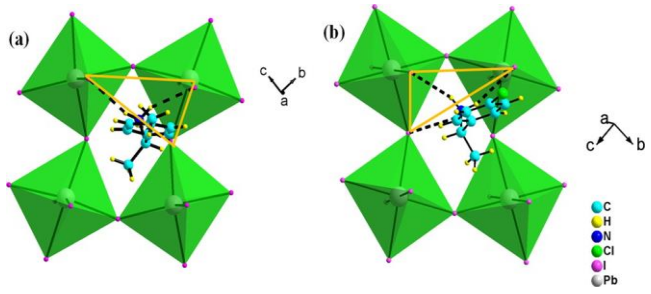

Figure 2. (a,b) Showing terminal halide and right-angled triangle bonding configuration in both MPEPI and CEPI, respectively.

The thin-film glancing angle X-ray diffraction (GAXRD) pattern shows strong orientation in both MPEPI- and CEPI- layered sheets along (2*l*00) and (00*l*) (*l* = 1,2,3..) directions, respectively, as shown in Figure 3. The corresponding *d*- spacing in MPEPI and CEPI are 16.25 and 16.89 Å, respectively, which are the same as observed from the single crystal diffraction analysis. As shown in Figure 3, the thin-film XRD is coinciding with the observed powder XRD extracted from the crystallographic information.

The thermogravimetry analysis (TGA) and the derivative thermogravimetry (DTG) curve of MPEPI (Figure 4a), the temperature up to which it is stable is observed to be 231 °C, suggests that both are thermally stable up to 240 °C with organic decomposed with a weight loss of 49.95%. After this, only PbI_2 remains in the sample. In case of CEPI (Figure 4b), it is suggested that it is thermally stable up to 240.6 °C. Below this temperature, the intermediate organic is stable and a weight loss of 50.48% (which is 1.893 mg out of 3.75 mg) is observed with further increase in temperature. This weight loss suggests complete decomposition of organic, leaving PbI_2 alone behind. The thermal stability suggests that both these hybrids can be used for device operations even up to 200 °C. Beyond this temperature, organic completely decomposes with a weight loss of 52.66% (which is 2.94 mg out of 5.7487 mg), leaving PbI_2 behind.

*Optical Absorption and PL Features of IO Hybrid.*These 2D IO hybrids are naturally self-assembled into alternative stacks of the PbI_6 infinitely extended network, where organic moieties are conformed within the layer spacing (Figure 1)., the Pb−I−Pb angles are observed to be ∼153.7 and ∼147.27° for CEPI and MPEPI, respectively (Figure 1). Therefore, it is obvious that the more crumpled (MPEPI) system shows UV side shift compared to the less crumpled CEPI system. If we compare with other 2D IO hybrids published previously,[23] $(4\text{-}ClC_6H_4NH_3)_2PbI_4$ (4- chloroanilinium tetraiodoplumbate, CAPI) is having a relatively more crumpling Pb−I−Pb angle (143.01°) with the corresponding PL peak at 484 nm, while $(C_6H_5C_2H_4NH_3)_2PbI_4$ (phenyl ethylammonium tetraiodo- plumbate, PAPI) is having a more planar arrangement with the Pb−I−Pb angle (155.43°) with red-end emission at 523 nm.

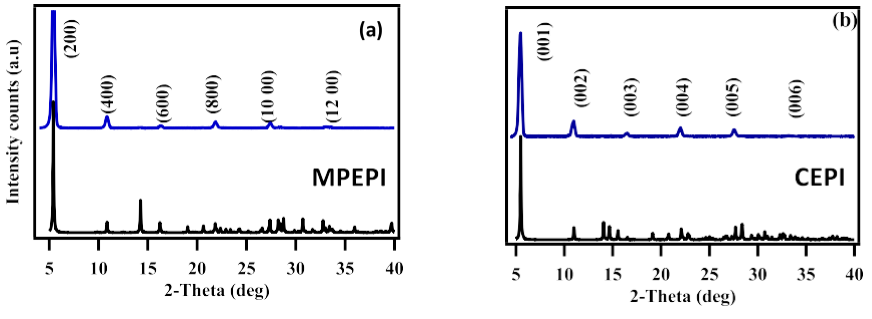

ISSN NO: 2770-0003
March 2024

Figure 3. (a,b) are the thin film glancing angle XRD (GAXRD) of MPEPI and CEPI (blue) and powder XRD (black) extracted from single crystal XRD data with the orientation on the substrate along (0,0,*l*) and (2*l*,0,0) (*l* = 1,2,3...) planes, respectively.

MPEPI CEPI

Figure 4. (a,b) shows the TGA (red) and DTG (blue) curves of MPEPI and CEPI, respectively.

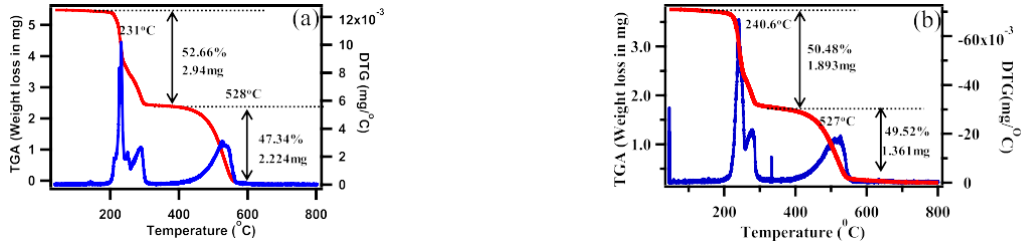

Figure 5. (a,b) shows the absorption and PL spectra of MPEPI and CEPI thin films respectivelyHigh-Resolution

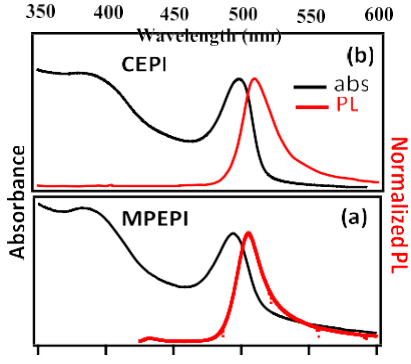

PL Imaging and Spectral Spatial Mapping of IO Hybrid Crystals.

Apart from structural variations, excitons from these 2D IO hybrids are highly sensitive to thickness. Typically, 2D alignment sustains to a thickness around 120 nm, beyond which crystal packing gets crumpled because of heaviness. Therefore, probing the crystal would be of worth to see the effect of crystal packing. However, probing with conventional excitation, above the band gap ($\hbar\omega \geq E_g$, 1PA-PL), is limited by the penetration depth ($1/\alpha_0$) which is few 100 s of nanometers, whereas, nonlinear pumping, that is, two- (or more) photon excitation ($2\hbar\omega \geq$ Eg, 2PA-PL) probes much deeper depths and gives a comprehensive idea of several excitons that are clearly PbI network order-/disorder-dependent.[23-24]

Figure 6 presents the 1PA-PL and 2PA-PL spectra of CEPI crystals. Here, for 1PA-PL excitations, 400 nm CW and 400 nm fs1 lasers and for 2PA-PL 800 nm, fs1 laser is used. The deconvoluted 1PA-PL spectra for both CW and fs1 400 nm excitations (Figure 7a,b) show three types of emission peaks: the strong and narrow dominant peak at 512 nm (fwhm ≈ 15 nm), a shoulder at 541 nm (fwhm ≈ 20 nm), and a broad weak shoulder at 585 nm (fwhm > 60 nm). The strong emission features at 512 nm is attributed to free excitons (PL_{FE}) which originates from the near-top surface. The shoulder peak at 541 nm is attributed to crumpled excitons (PL_{CE}) and the broad emission at 585 nm is for defect induced broad emission (PL_{def}), respectively. In general, both the spectra (Figure 6a,b) are dominated by the strong green emission at 512 nm and a shoulder at 541 nm.

ISSN NO: 2770-0003
March 2024

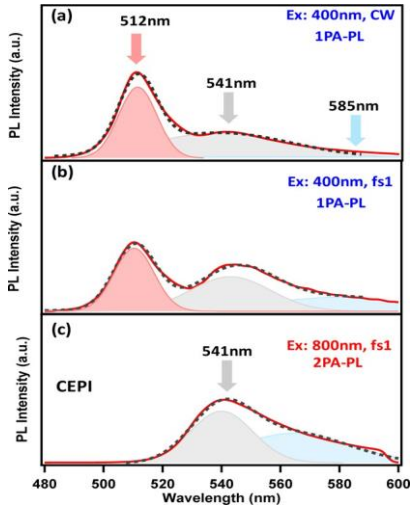

Figure 6. (a) shows 1PA-PL spectra of CEPI crystal when excited by 400 nm CW laser. The spectra are deconvoluted into free exciton (PL_{FE}) at 512 nm, crumpled exciton (PL_{CE}) at 541 nm, and defect- induced emission (PL_{def}) at 585 nm. Similarly, (b,c) shows 1PA-PL and 2PA-PL spectra under 400 and 800 nm (from fs1 laser) excitations, respectively.

Conclusions. Two new 2D IO-layered hybrid semiconductors $(R{-}C_6H_4C_2H_4NH_3)_2PbI_4$ (R = CH_3, Cl) are successfully synthesized and their crystal structures have been analyzed. Both are self-assembled into alternative stacks of a two- dimensionally extended PbI_6 network, where the two organic moieties are interdigitized as spacers. These single crystals are thermally much stable for more than 200 °C. As a virtue of dielectric contrast and quantum confinement-related effects, these 2D IO hybrid semiconductors show strong room- temperature Mott type exciton PL with high binding energies greater than 200 meV and the order of magnitude greater than their parent PbI_2 (~23 meV). In the thin-film form, they are perfectly oriented along the *c*-axis. The strong room-temperature exciton emission features are highly sensitive to the local environment and crystal packing. The spectral, imaging, and spatial mapping studies of single crystals revealed many interesting details about their self-assembly, crystal packing, and local environment. The comparison between the linear and nonlinear optical excitation imaging and spatial mapping of single crystal studies reveal the fact that two different types of excitons are present in these systems. The conventional one- photon absorption-induced PL (UV-excited, $E_{exe} = \hbar\omega \geq E_g$, 1PA-PL) probing is restricted by shorter penetration depths ($1/\alpha_0$) and reveals free-exciton emission originated from perfectly aligned 2D self-assembly from the top few layers, whereas the two-photon absorption-related excitation (infrared excited, $E_{exe} = 2\hbar\omega \geq E_g$, 2PA-PL) probes much deeper depths of the crystal and demonstrates entirely different excitons, which are energy down-shifted excitons, originated from the locally crumpled layered arrangement. The room-temperature exciton features and one- and two-photon imaging/spatial mapping studies further pave way to explore these stable 2D IO semiconductors for many new optoelectronic applications.

References.

1. Ishihara, T.; Takahashi, J.; Goto, T. Optical properties due to electronic transitions in two-dimensional semiconductors $(C_nH_{2n+1}NH_3)_2PbI_4$. Phys. Rev. B: Condens. Matter Mater. Phys. 1990, 42, 11099.
2. Guloy, A. M.; Tang, Z.; Miranda, P. B.; Srdanov, V. I. A new luminescent organic-inorganic hybrid compound with large optical nonlinearity. Adv. Mater. 2001, 13, 833−837.
3. Pradeesh, K.; Yadav, G. S.; Singh, M.; Vijaya Prakash, G. Synthesis, structure and optical studies of inorganic-organic hybrid semiconductor, $NH_3(CH_2)_{12}NH_3PbI_4$. Mater. Chem. Phys. 2010, 124, 44−47.
4. Mitzi, D. B. A Layered Solution Crystal Growth Technique and the Crystal Structure of $(C_6H_5C_2H_4NH_3)_2PbCl_4$. J. Solid State Chem. 1999, 145, 694−704.
5. Calabrese, J.; Jones, N. L.; Harlow, R. L.; Herron, N.; Thorn, D. L.; Wang, Y. Preparation and Characterization of Layered Lead Halide Compounds. J. Am. Chem. Soc. 1991, 113, 2328−2330.

ISSN NO: 2770-0003
March 2024

6. Xu, Z.; Mitzi, D. B.; Dimitrakopoulos, C. D.; Maxcy, K. R. Semiconducting perovskites (2-$XC_6H_4C_2H_4NH_3)_2SnI_4$ (X = F, Cl, Br): Steric interaction between the organic and inorganic layers. Inorg. Chem. 2003, 42, 2031−2039.
7. Kulicka, B.; Jakubas, R.; Ciunik, Z.; Bator, G.; Medycki, W.; Świergiel, J.; Baran, J. Structure, phase transitions and molecular dynamics in 4-methylpyridinium tetrachloroantimonate(III), [4-$CH_3C_5H_4NH][SbCl_4]$. J. Phys. Chem. Solids 2004, 65, 871−879.
8. Billing, D. G.; Lemmerer, A. Synthesis, characterization and phase transitions in the inorganic-organic layered perovskite-type hybrids $[(C_nH_{2n+1}NH_3)_2PbI_4]$, n = 4, 5 and 6. Acta Crystallogr., Sect. B: Struct. Sci. 2007, 63, 735−747.
9. Billing, D. G.; Lemmerer, A. Inorganic−organic hybrid materials incorporating primary cyclic ammonium cations: The lead iodide series. CrystEngComm 2007, 9, 236−244.
10. Billing, D. G.; Lemmerer, A. Inorganic-organic hybrid materials incorporating primary cyclic ammonium cations: The lead bromide and chloride series. CrystEngComm 2009, 11, 1549−1562.
11. Liu, Y.; Yang, P.; Meng, J. Synthesis, crystal structure and optical properties of a novel organic-inorganic hybrid materials $(C_9H_{14}N)_2PbCl_4$. Solid State Sci. 2011, 13, 1036−1040.
12. Park, S.-H.; Oh, I.-H.; Park, S.; Park, Y.; Kim, J. H.; Huh, Y.-D. Canted antiferromagnetism and spin reorientation transition in layered inorganic-organic perovskite $(C_6H_5CH_2CH_2NH_3)_2MnCl_4$. Dalton Trans. 2012, 41, 1237−1242.
13. Papavassiliou, G. C.; Koutselas, I. B.; Terzis, A.; Whangbo, M. H. Structural and electronic properties of the natural quantum-well system $(C_6H_5CH_2CH_2NH_3)_2SnI_4$. Solid State Commun. 1994, 91, 695−698.
14. Mitzi, D. B.; Wang, S.; Feild, C. A.; Chess, C. A.; Guloy, A. M. Conducting layered organic-inorganic halides containing <110>- oriented perovskite sheets. Science 1995, 267, 1473
15. Hong, X.; Ishihara, T.; Nurmikko, A. V. Dielectric confinement effect on excitons in PbI4-based layered semiconductors. Phys. Rev. B: Condens. Matter Mater. Phys. 1992, 45, 6961−6964.
16. Mitzi, D. B. Synthesis, crystal structure, and optical and thermal properties of $(C_4H_9NH_3)_2MI_4$ (M= Ge, Sn, Pb). Chem. Mater. 1996, 8, 791−800.
17. Fujisawa, J.-I.; Ishihara, T. Charge-transfer transitions between wires and spacers in an inorganic-organic quasi-one-dimensional crystal methylviologen lead iodide. Phys. Rev. B: Condens. Matter Mater. Phys. 2004, 70, 113203.
18. Kawano, N.; Koshimizu, M.; Asai, K. The effect of Wannier and Frenkel exciton resonance on the luminescence properties of organic-inorganic layered perovskite-type compounds. J. Phys. Chem. C 2012, 116, 22992−22995.
19. Pradeesh, K.; Nageswara Rao, K.; Vijaya Prakash, G. Synthesis, structural, thermal and optical studies of inorganic-organic hybrid semiconductors, R-PbI_4. J. Appl. Phys. 2013, 113, 083523.
20. Takahashi, Y.; Obara, R.; Lin, Z.-Z.; Takahashi, Y.; Naito, T.; Inabe, T.; Ishibashi, S.; Terakura, K. Charge-transport in tin-iodide perovskite $CH_3NH_3SnI_4$: Origin of high conductivity. Dalton Trans. 2011, 40, 5563−5568.
21. Prakash, G. V.; Pradeesh, K.; Ratnani, R.; Saraswat, K.; Light, M. E.; Baumberg, J. J. Structural and optical studies of local disorder sensitivity in natural organic−inorganic self-assembled semiconductors. J. Phys. D: Appl. Phys. 2009, 42, 185405.
22. Zhang, S.; Lanty, G.; Lauret, J.-S.; Deleporte, E.; Audebert, P.; Galmiche, L. Synthesis and optical properties of novel organic-inorganic hybrid nanolayer structure semiconductors. Acta Mater. 2009, 57, 3301−3309.
23. Kagan, C. R.; Mitzi, D. B.; Dimitrakopoulos, C. D. Organic-inorganic hybrid materials as semiconducting channels in thin-film field-effect transistors. Science 1999, 286, 945−947.
24. Mitzi, D. B.; Dimitrakopoulos, C. D.; Kosbar, L. L. Structurally tailored organic-inorganic perovskites: Optical properties and solution-processed channel materials for thin-film transistors. Chem. Mater. 2001, 13, 3728−3740.
25. Mitzi, D. B.; Dimitrakopoulos, C. D.; Rosner, J.; Medeiros, D. R.; Xu, Z.; Noyan, C. Hybrid field-effect transistor based on a low-temperature melt processed channel layer. Adv. Mater. 2002, 14, 1772−1776.